

Earth and Space Science



RESEARCH ARTICLE

10.1029/2023EA002934

Key Points:

- A low-cost 3-component seismometer has been tested for passive shallow applications
- The seismometer has non-linear response for high-amplitude (mm/s) excitation signals
- Lab and field tests confirm the -3 dB band ranges from 0.7 to 39 Hz and an offset of about 0.5 s was found in the filed data whose timing was provided by a USB GPS antenna

Correspondence to:

D. Arosio,
diego.arioso@unimore.it

Citation:

Arosio, D., Aguzzoli, A., Zanzi, L., Panzeri, L., & Scaccabarozzi, D. (2023). Lab and field tests of a low-cost 3-component seismometer for shallow passive seismic applications. *Earth and Space Science*, 10, e2023EA002934. <https://doi.org/10.1029/2023EA002934>

Received 13 MAR 2023

Accepted 16 AUG 2023


Author Contributions:

Conceptualization: D. Arosio, D. Scaccabarozzi
Data curation: D. Arosio, A. Aguzzoli, L. Panzeri
Formal analysis: D. Arosio, L. Zanzi, D. Scaccabarozzi
Investigation: A. Aguzzoli, L. Panzeri, D. Scaccabarozzi
Methodology: D. Arosio, A. Aguzzoli, D. Scaccabarozzi
Software: D. Arosio, A. Aguzzoli
Supervision: D. Arosio, D. Scaccabarozzi
Validation: D. Arosio, L. Zanzi
Writing – original draft: D. Arosio

© 2023 The Authors. Earth and Space Science published by Wiley Periodicals LLC on behalf of American Geophysical Union.

This is an open access article under the terms of the [Creative Commons Attribution-NonCommercial-NoDerivs License](https://creativecommons.org/licenses/by-nc-nd/4.0/), which permits use and distribution in any medium, provided the original work is properly cited, the use is non-commercial and no modifications or adaptations are made.

Lab and Field Tests of a Low-Cost 3-Component Seismometer for Shallow Passive Seismic Applications

D. Arosio¹ , A. Aguzzoli¹, L. Zanzi², L. Panzeri², and D. Scaccabarozzi³

¹Department of Chemical and Geological Sciences, Università degli Studi di Modena e Reggio Emilia, Modena, Italy,

²Department of Civil and Environmental Engineering, Politecnico di Milano, Milano, ITALY, ³Department of Mechanics, Politecnico di Milano, Milano, Italy

Abstract We performed laboratory tests and field surveys to evaluate the performance of a low-cost 3-component seismometer, consisting of three passive electromagnetic spring-mass sensors, whose 4.5 Hz natural frequency is extended down to 0.5 Hz thanks to hyper damping. Both lab and field datasets show that the -3 dB band of the seismometer ranges approximately from 0.7 to 39 Hz, in agreement with the nominal specifications. Median magnitude frequency response curves obtained from processing field data indicate that lower corner of the -3 dB band could be extended down to 0.55 Hz and the nominal sensitivity may be overestimated. Lab results confirm the non-linear behavior of the passive spring-mass sensor expected for high-level input signals (a few to tens of mm/s) and field data confirm relative timing accuracy is ± 10 ms (1 sample). We found that absolute timing of data collected with USB GPS antennas can be affected by lag as large as $+0.5$ s. By testing two identical units, we noticed that there could be differences around 0.5 dB (i.e., about 6%) between the components of the same unit as well as between the same component of the two units. Considering shallow passive seismic applications and mainly focusing on unstable slope monitoring, our findings show that the tested seismometer is able to identify resonance frequencies of unstable rock pillars and to generate interferograms that can be processed to estimate subsurface velocity variations.

Plain Language Summary This study describes some tests that we did to evaluate a seismometer that is cheaper than similar products on the market. A seismometer is able to sense and collect seismic waves and can be used for several applications including global seismology and hydrocarbon exploration. In our work, we consider passive seismic applications, that is, we focus on seismic waves generated by non-controlled sources (aka seismic noise). Either the seismic sources are natural or man-made, a valuable seismometer should allow to record weak signals in a wide frequency band, especially at relatively low frequency (<5 Hz). The results of our tests show that the cheap seismometer can record frequencies down to approximately 0.5 Hz, while, to keep costs low, the highest frequency is limited to about 40 Hz. Field tests show that the seismometers can retrieve information from seismic noise as weak as a few micrometers per second, while lab test with higher inputs shows that the response of the seismometer is dependent upon the input velocity. Overall, we found that the nominal specifications of the seismometers are met, thus the tested unit is a valuable tool for shallow passive-seismic applications with relatively-low-frequency, low-amplitude signals, and a limited budget.

1. Introduction

The Passive seismic techniques have become increasingly appealing in the last decades chiefly because they do not require active sources and great amounts of information can be extracted by the so-called seismic noise. Ambient vibrations are generated either by natural or manmade sources generally placed at or close-to the Earth's surface. Therefore, the passive seismic wavefield primarily consists of surface waves, though the proportion between Rayleigh and Love waves, as well as between surface and body waves, may vary significantly from site to site (Bonney-Claudet et al., 2006). With respect to active sources, the spectrum of seismic noise is appreciably shifted toward lower frequencies, with natural phenomena (mainly ocean waves and meteorological events) and anthropogenic activities (e.g., industrial machineries and road traffic) generating frequencies below and above 1 Hz, respectively (Bonney-Claudet et al., 2006). Recorded amplitudes are typically on the order of a few to hundreds of $\mu\text{m/s}$, obviously excluding close-range transients.

The ambient seismic noise collected with either single-station or array recordings is used in different shallow geophysical methodologies (Larose et al., 2015). The horizontal-to-vertical spectral ratio (HVSR) of 3-component

Writing – review & editing: D. Arosio, A. Aguzzoli, L. Zanzi, L. Panzeri, D. Scaccabarozzi

(3C) single-station data is either an active or, more often, a passive seismic methodology that has been extensively used in the past 30 years for site effect evaluation (Nakamura, 2019). More recently, 3C passive surveys with stand-alone seismometers have addressed unstable slopes and rock blocks by analyzing both spectral and polarization features with diverse algorithms in order to monitor phenomena of directional amplification associated to vibration modes of the investigated structures (Bottelin et al., 2017; Kleinbrod et al., 2017; Taruselli et al., 2021). Passive array techniques typically rely on the collection and processing of Rayleigh waves (usually their vertical component only), whose dispersion curves are inverted to estimate the 1D shear-wave velocity model of the subsurface (Foti et al., 2018). Several approaches have been proposed in the scientific literature, such as the spatial autocorrelation method (SPAC; Okada, 2003), the refraction microtremor method (REMI; Louie, 2001) and the passive multichannel analysis of surface waves (passive MASW; Park et al., 2005). Seismic noise interferometry (SNI) can also be considered as an array technique, though just two receivers are needed to collect and process ambient vibration data (Garambois et al., 2019) and can be used to retrieve either surface-wave transmission responses or exploration reflection responses (Wapenaar et al., 2010). In addition, coda wave interferometry (CWI) makes use of strongly scattered waves to perform interferometric measurements of temporal changes in the medium (Snieder, 2006), for instance variations in seismic velocity due to fluid saturation changes (Mainsant et al., 2012). Le Breton et al. (2021) recently presented a thorough review about landslide monitoring with CWI, and Larose et al. (2015) have described other near-surface passive seismics applications, including monitoring building modal frequencies and estimation of bedload transport by analyzing river-induced noise.

All the applications described above may be further developed and tuned, especially if seismometers with proper features, mainly low natural frequency (<1 Hz) and low self-noise, are available at low cost. This is particularly true in the case of spatially dense surveys where many recording stations are required to produce detailed subsurface 2D/3D images. Rugged and easy-to-handle stand-alone receivers can obviously ease field operations, especially in densely urbanized or very inaccessible rural areas, with broadband and large dynamic range being obviously a plus.

In this work we present our study regarding lab and field testing of a low-cost 3C seismometer that could foster the development of shallow passive seismic applications. Recently, this unit, or similar ones produced by the same manufacturer, have been employed for different aims, including studying global quieting of seismic noise during COVID-19 pandemic lockdown (Lecocq et al., 2020), densification of seismic networks with the so-called citizen Seismology (Calais et al., 2022; Walter et al., 2019), monitoring of rockfalls (Manconi et al., 2018), induced seismicity (Hicks et al., 2019), icequakes (Winter et al., 2021) and structural health (Alarcón et al., 2023; Özcebe et al., 2022). Anthony et al. (2019) have analyzed the performance of a seismic station similar to the one considered here, though addressing seismological applications. They found sensitivity within 10% (i.e., approximately 0.9 dB) of nominal, NTP timing errors no greater than 20 ms, but high self-noise compared to intermediate period sensors. They conclude that this seismic station is a possible candidate for densification of seismic network targeted at recording local or regional events, but claim it is not suitable for studies using ambient seismic noise. In this study, we propose a different characterization methodology, both in lab and in the field, and consider shallow passive seismic applications, mainly addressing the monitoring of rock structures, whose stability is related to their vibration modes, and of subsurface fluid saturation changes, that in turn cause seismic velocity variations.

2. Seismometers

Here we analyze the performance of the Raspberry Shake seismometer. More in detail, we focus on the release V5 (firmware version 0.18, then updated to 0.20) of the 3D version (RS3D hereafter) of this seismic station that integrates three orthogonally-placed 4.5 Hz electromagnetic geophones, the digitizers and an embedded PC into a single enclosure (IP10 or IP67). The sampling frequency is fixed to 100 Hz and the corner frequency of the sensing elements, whose original natural frequency is 4.5 Hz, is electronically extended down to 0.5 Hz thanks to hyper damping (Lippmann & Gebrande, 1983). Accordingly, the nominal -3 dB bandwidth ranges from 0.7 to 39 Hz (Table 1). Additional features are the 5 V power supply voltage, the 8 GB expandable memory to record data in miniSEED format and the Wi-Fi connection to send data to a remote device. Unit timing is based on the Network Time Protocol (NTP) providing 1 sample of accuracy, that is, ± 10 ms at 100 Hz. However, when no internet connection is available, for example, during field surveys, it is possible to get the timing with the same accuracy through a GPS module connected to the USB port.

For comparison purposes, we also used the Nanometrics Trillium Compact 20s seismometer together with the associated Centaur digitizer. This system (NT20 hereafter) could be considered as a reference since it is

Table 1
Main Nominal Specifications of RS3D and NT20 Seismic Stations

	RS3D (V5)	NT20 [Centaur: 3 channels; gain 0 dB; input range 40 V peak-to-peak; GPS duty-cycled]
Bandwidth (−3 dB)	0.7–39 Hz	0.05–108 Hz
Sensitivity	3.61×10^8 counts/(m/s)	753.1 V/(m/s) (sensor) 4×10^5 counts/V (digitizer) 3.01×10^8 counts/(m/s) (sensor + digitizer)
Sampling frequency	100 Hz (fixed)	From 1 to 5,000 Hz (selectable)
Timing accuracy	± 10 ms (1 sample) (NTP and GPS)	< 100 μ s
Digitizer and dynamic range	24-bit ADC Sigma-Delta 124 dB @ 100 sps from 1 to 20 Hz (entire analog to digital hardware chain)	True 24-bit ADC > 152 dB @ 1 Hz (sensor) 142 dB @ 100 sps (digitizer) 1.7 μ V @ 100 sps (digitizer)
Minimum Detection Threshold (estimate)	0.03 μ m/s RMS from 1 to 20 Hz @ 100 sps	
Clip level	± 23.3 mm/s (0.1–10 Hz) (estimate)	± 26 mm/s (0.1–10 Hz) and 0.17 g above 10 Hz (sensor)
Power Consumption	1.6 W (estimate)	± 20.97 V (digitizer) 0.195 W typical (sensor) 1 W (digitizer)
Cost	~1 k€	~15 k€

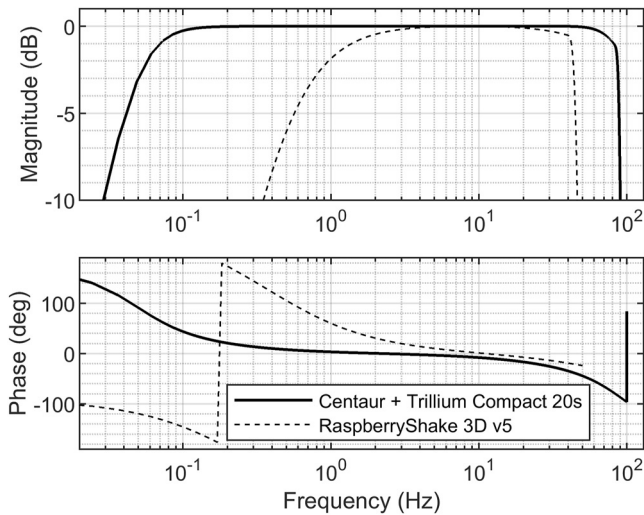


Figure 1. RS3D and NT20 normalized magnitude and phase frequency response functions. Centaur data logger is considered to have 200 Hz sampling frequency, 0 dB gain, 40 V peak-to-peak input range and 0.001 Hz high-pass filter with linear phase.

widespread in broadband seismological surveys (Anthony et al., 2019). The seismometer features a symmetric triaxial force feedback sensor, with the force provided by a capacitive transducer, having a -3 dB band spanning from 0.05 to about 108 Hz (Table 1) and sampling frequency adjustable from 1 up to 5,000 Hz. Also digitizer gain and input range can be set in order to control the overall system sensitivity. Time synchronization is provided by the Precision Time Protocol (PTP), but, as for the RS3D, it is also possible to use a GPS antenna in the field to improve timing accuracy. For additional information and for a comparison of the main features of the considered seismic stations, the reader can refer to Table 1, while Figure 1 depicts amplitude and phase of the FRF of both units (Templeton, 2017; <https://manual.raspberyrshake.org/metadata.html#raspberry-shake-rs3>).

RS3D is approximately one order of magnitude cheaper than NT20 (i.e., about a thousand vs. ten thousand euros) and the cost may vary depending on whether a GPS antenna and all-weather enclosures are purchased for the unit. However, RS3D may have some drawbacks that are due to the fact that its sensing elements (i.e., electromagnetic velocimeters) are actually passive inertial sensors consisting of a damped spring-mass system. When considering recording low-frequency ground motion, the main disadvantages of passive seismometers are (Ackerley, 2015): (a) large masses and compliant suspensions are needed to have satisfactory sensitivity at low frequencies, making the system difficult to handle and susceptible to damage; (b) the spring and

the velocimeter can have a non-linear behavior dependent upon the displacement of the proof mass from the rest position; (c) there are conflicting damping requirements in that damping must be low to minimize self-noise, but high enough to limit resonance at the natural frequency of the system. Although the above-mentioned issues are partly tackled thanks to the hyper damping, it is interesting to evaluate the performance of RS3D with respect to NT20, especially for low-frequency (<2 Hz) and relatively high-amplitude (\sim mm/s) input signals.

3. Seismometer Testing

3.1. Laboratory Tests

We carried out dynamic characterization tests of two RS3D and two NT20 seismometers and placed them on a vibrating table to estimate the RS3D's amplitude frequency response function (FRF). We set input signal values higher than seismic noise generally recorded in the field to investigate possible nonlinearities affecting the tested sensors, especially the passive ones. The testing facility (Figure 2) comprised a vertical shaker (TIRA Vib shaker) operated in an open loop using an Agilent signal generator (33210A type) and a laser Doppler vibrometer (LDV—Polytech OFV 505) pointed at the case of the sensor mounted on the shaker in order to measure its velocity with high accuracy and large bandwidth. During the tests, the sampling frequency of the LDV was generally set at 2 kHz.

Laboratory tests initially involved logarithmic sweep sine excitation between 0.5 and 40 Hz over 60 s to investigate the entire RS3D nominal bandwidth (Figures 3a and 3b). Each test typically involved at least three consecutive sweep signals. We set excitation amplitudes between 10 and 30 mV, resulting in input rms and peak velocity values, as detected by the LDV, ranging approximately from 2 to 9 mm/s and from 4 to 19 mm/s, respectively. The processing sequence involved upsampling seismometer data to LDV sampling frequency, zero-phase IIR 0.3 Hz high-pass filtering, time alignment of seismometer and LDV data with cross correlation followed by time cut to a common time window, whose edges were tapered with a cosine function. To estimate amplitude spectra, we resorted to a non-parametric spectral estimation technique, namely the multitaper method (Thomson, 1982), that

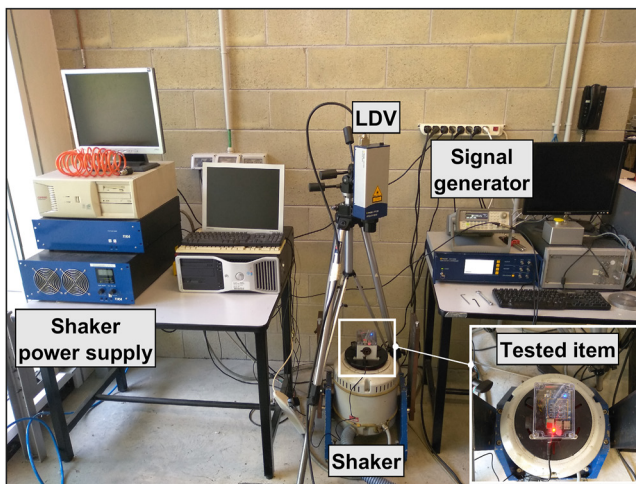


Figure 2. Setup of the laboratory test. The image depicts the test of a RS3D that is placed onto the vertical shaker; the Laser Doppler Vibrometer points at the RS3D (lower-right inset) to record the reference excitation.

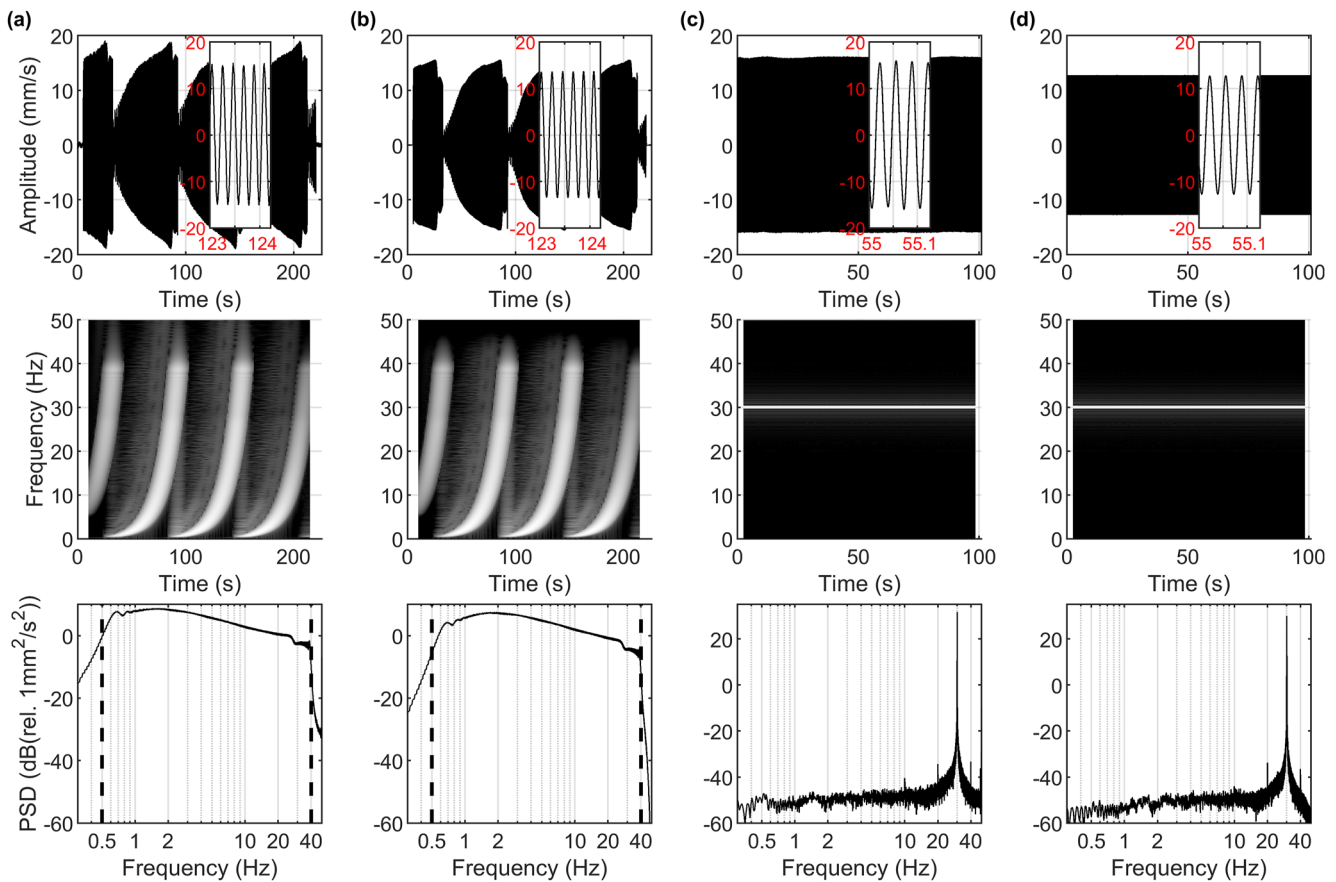


Figure 3. Examples of lab test results. (a) Sweep signal collected by the LDV with 30 mV excitation amplitude (top), its normalized spectrogram (middle; 20 s windows with 95% overlapping) and the multitaper spectral estimate (bottom) with dashed vertical lines limiting the sweep bandwidth. Panel (b) same as (a) but for RS3D. (c) 30 Hz signal collected by the LDV with 30 mV excitation amplitude (top), its normalized spectrogram (middle; 5 s windows with 95% overlapping) and the multitaper spectral estimate (bottom). Panel (d) same as (c) but for RS3D. Insets in the top figures are zoomed windows of the collected signals.

makes use of orthogonal data tapers to reduce bias and variability in the final estimate. In more detail, we set the parameters of the computation to obtain amplitude spectra with 0.05 Hz frequency resolution and this resulted in the use of 19 orthogonal tapers, two of which were eventually discarded to retain only the ones with optimal frequency concentration in the specified resolution bandwidth. Finally, the ratio between the seismometer and the LDV amplitude spectra yields the modulus of the seismometer FRF.

The RS3D seismometers were additionally tested with monochromatic sinusoidal signals (step sine test) to further explore the dynamic behavior of the RS3D, especially at frequencies close to the limits of the -3 dB nominal bandwidth (Table 1). We tested twelve different frequencies, that is, 0.6, 0.7, 0.8, 1, 2, 10, 20, 30, 35, 38, 39, 40 Hz, with durations of approximately 100 s and RMS amplitudes similar to the sweep ones (Figures 3c and 3d). Because the shaker operated in an open loop, it has to be noted that excitation amplitudes generally increased with the frequency of the monochromatic signal. The test set up and data processing are the same described above.

Despite the high-amplitude excitation levels, the results of the dynamic characterization confirm that the amplitude FRFs of RS3D vertical geophones are in agreement with the nominal specifications, with a -3 dB bandwidth within the 0.7–39 Hz range for both the sweep and the monochromatic input signals with different excitation amplitudes (Figure 4a). However, the magnitude response tends to be lower (up to about -2 dB) than the nominal one close to the upper limit of the band. In addition, two points are worthwhile noticing. First, velocity inputs being similar, the RS3Ds show responses having different amplitudes, with larger mean differences of about 0.4 dB observed in the 2–30 Hz band. Second, variations in the excitation signals highlighted the non-linear behavior of the RS3D, with lower values of the FRF obtained with higher rms input velocity and differences as large as 0.6 dB observed in the -3 dB band. We think that this behavior is due to the mechanical characteristics of

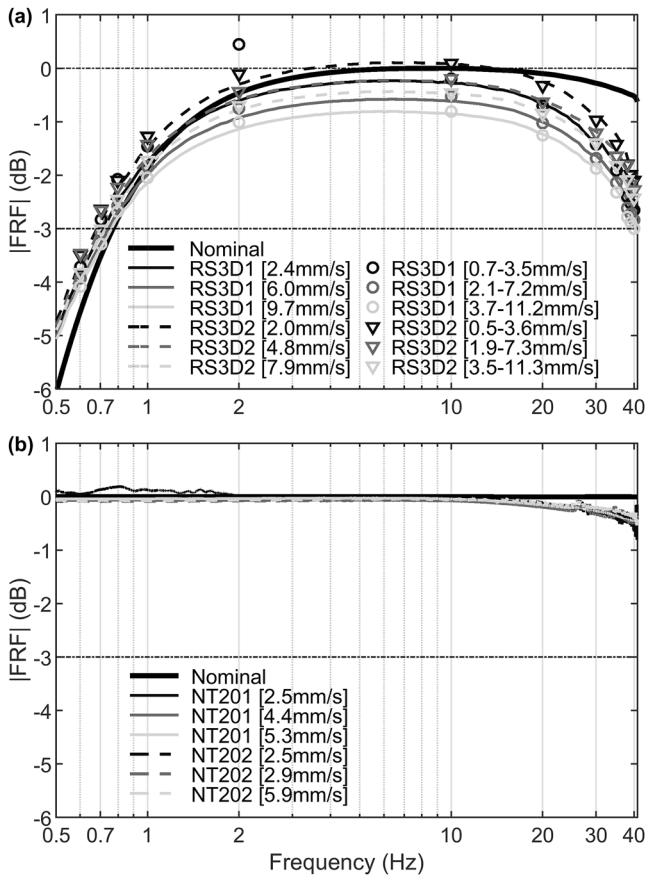


Figure 4. Amplitude frequency response functions obtained in the lab with RS3D (a) and NT20 (b) seismometers (vertical component). In (a), lines and markers represent results obtained with the sweep and sinusoidal excitations, respectively. Thick solid black lines are the nominal responses (Figure 1) and dash-dotted horizontal lines are the -3 dB level; velocity values are rms values of each test.

spring-mass system of the passive geophone sensor, as stated previously and in other studies (Barzilai et al., 1998; Oome et al., 2009; Stoll, 2015). On the contrary, the NT20s reveal nearly flat FRFs in the tested bandwidth for all the excitation amplitude levels (Figure 4b), in accordance with the specifications that indicate high-frequency response within 1 dB of nominal up to 45 Hz.

No phase response was estimated in the lab tests because it is not possible to connect the RS3D and the LDV to a single acquisition board, with common reference clock and sampling frequency.

3.2. Field Acquisitions

Measurements in the field were performed to evaluate the performance of the RS3D in temporary field installations (Figure 5), considering 3C acquisitions of seismic signals with amplitudes typically lower than the ones tested in the lab as well as with more energy at lower frequencies. The same RS3Ds tested in the lab and different NT20s were deployed at different sites, mainly consisting of potentially unstable rock blocks and pillars in northern Italy and Malta (Arosio et al., 2019; Taruselli et al., 2019). In addition, seismic stations have also been occasionally installed at sites where groundwater pumping tests were ongoing (Ventasso (RE, Italy) test site; Taruselli et al., 2020a) or across slopes showing either significant or negligible displacements (Ca' Lita earth flow (RE, Italy); Taruselli et al., 2020b; Aguzzoli et al., 2021). Deployed units have always been equipped with a GNSS receiver so that a common accurate time reference is available. Nominal RS timing accuracy is ± 1 sample at 100 Hz sampling frequency, that is 10 ms (Table 1), while the Nanometrics timing accuracy is < 0.1 ms (with GPS power mode set to duty cycled). Different coupling systems were used depending on the different conditions of the investigated sites. Whenever topsoil was present, spikes nearly 7 cm long were generally preferred, even in rock block monitoring. Otherwise, leveling screws were used. Alignment of sensors in the horizontal plane was obtained with a digital compass, while their verticality was checked by means of the bull's eye spirit level mounted on the case of all the seismometers. Overall, for our comparison, we considered data collected in 6 different sites and approximately 65 hr of field measurements.

Based on the outcomes of the previously described laboratory tests, we evaluate the performance of the RS3Ds considering the data collected by the NT20s as a reference. The pre-processing sequence described in the following applies to couple of seismic stations that were installed in the field close to one another. First, the initial 15 min or more of the collected time series have been discarded in order to consider sensor stabilization after

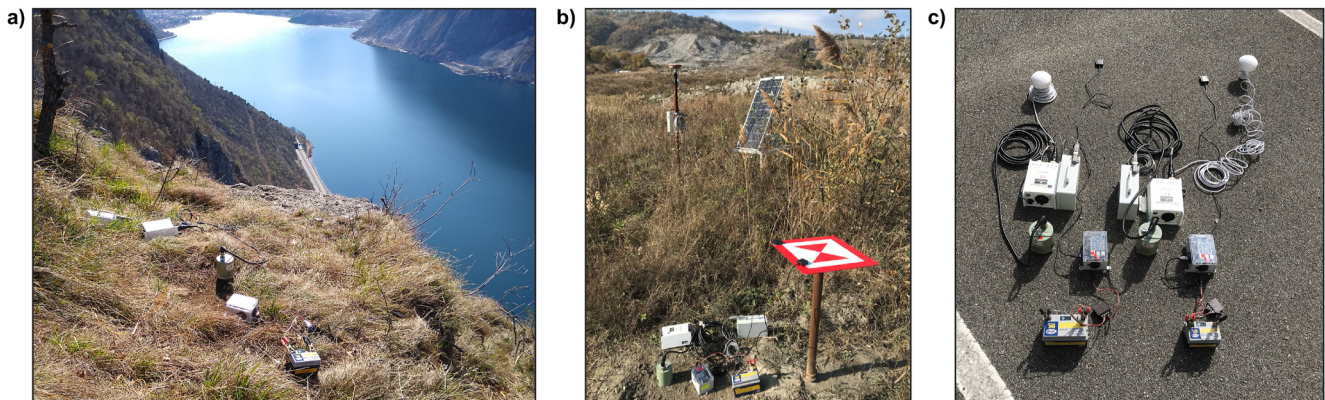


Figure 5. Field tests performed by deploying RS3Ds and NT20s on top of an unstable rock pillar (a), on a slope affected by an earth flow (b) and on asphalt (c).

field deployment. Especially for the NT20, continuous quality data are available within minutes of deployment with no requirement for further intervention. Likewise, the last part of the recording was eliminated to get rid of the close-range high-amplitude signals and other artifacts generated by the field technicians when switching off the units. Second, signals were resampled to a common sampling frequency. In our case, considering that the RS and Trillium sampling frequencies were set to 100 and 200 Hz, respectively (Table 1), we resampled the raw time series by means of sinc interpolation to 1,000 Hz. This allows us to set a common initial time independently of when the two seismic stations started recording. After resampling, signals of the two seismometers could be perfectly aligned and cut over a common time interval and they were subsequently decimated to 200 Hz to limit the computational costs of the following steps. Finally, signals were band-pass filtered with a zero-phase IIR filter in the band 0.7–39 Hz to reject low-frequency high-amplitude signals and to focus the evaluation within the –3 dB band of the RS3D validated previously.

We used the accurate GNSS time reference to evaluate any possible time delays between the two tested seismic stations that we could not appraise with the lab tests. We resorted to normalized cross correlation that is routinely used in countless applications to determine the time lag between two signals and to evaluate their similarity in terms of waveforms. Unsurprisingly, cross correlation easily identified anomalous lags whenever one of the two tested units experienced issues with the locking to the GNSS network. Overall, we observed a positive lag of nearly 0.5 s meaning RS3Ds are delayed with respect to NT20s. This was also confirmed by an additional test in which we deployed the seismic stations on asphalt one next to the other (Figure 5c). In this test, pairwise cross correlation between components of the same seismometer type indicates lags are always zero, with normalized cross correlation (x y z) peak values (0.90 0.90 0.91) for RS3D and (0.74 0.65 0.97) for NT20. To investigate whether the observed systematic lag could be due to the phase spectra of the seismometers (Figure 1), we slightly modified the pre-processing sequence described above. In more detail, simple band-pass filtering was discarded and Nanometrics data were first deconvolved by Centaur Digitizer and Trillium sensor frequency responses (Templeton, 2017, p. 10% pre-whitening was applied to avoid boosting low frequencies excessively) and subsequently convolved with the RS one (Figure 1). However, no appreciable differences were obtained, and the systematic lag was still observed. Moreover, the delay is also found in the comparison of raw time series, so that we can confirm that the processing sequence we applied does not introduce any artifacts.

As far as cross correlation peak values are concerned, differences between band-pass filtered and deconvolved data have mean value around 20%. Generally, higher peak values are observed for the vertical component probably because of inaccurate alignment of the sensors in the horizontal plane. It was observed that low normalized peak values are obtained in case collected signals are disturbed by several high-amplitude transients (e.g., generated by operators on site).

Data collected in the field with the different seismometers were obviously compared also in terms of amplitude spectra. Pre-processing steps like the ones described above were applied, however no convolution/deconvolution was performed. Instead, time series were high-pass filtered with a 0.05 Hz zero-phase IIR filter and passband ripple of 0.1 dB and then converted from counts to physical units considering the maximum sensitivity estimated from the nominal transfer functions of the seismometers (i.e., $3.6150 \cdot 10^8$ counts/(m/s) for RS3D and $3.0124 \cdot 10^8$ counts/(m/s) for NT20; Table 1). In addition, signals collected by seismic stations pairs were time aligned by delaying RS data considering the median lag value estimated previously for the vertical component, that is, 0.48 s, except for data affected by GPS issues that were corrected for the median value of delays computed for the three components. The multitaper method was again used to estimate amplitude spectra, and, for statistical robustness of the comparison, the collected time series were divided in 200s-long time windows (T_w) and multitaper estimation was applied to each of them. The length of the selected time window should guarantee accurate spectral estimation down to frequency of 0.05 Hz, obtained with the relationship $10/T_w$ (McNamara & Buland, 2004). Finally, we computed component-wise spectral ratios (RS3D/NT20) for each analyzed couple of seismic stations deployed at different sites, after the estimated spectra were smoothed with the frequency-dependent averaging function proposed by Konno and Ohmachi (1998).

Figure 6 illustrates the results obtained for the two tested RS3Ds in the 0.2–45 Hz band. Ratios are expressed in decibel and presented in terms of relative probability, that is, for each frequency, the values of the estimated amplitude spectra are partitioned into bins (from –0.025 to 2.525 with step 0.05) and the value of each bin is the ratio between the number of elements in the bin and the total number of elements (i.e., the sum of all the bin values gives unity). The images also show the median spectral ratio, together with the 25th and the 75th

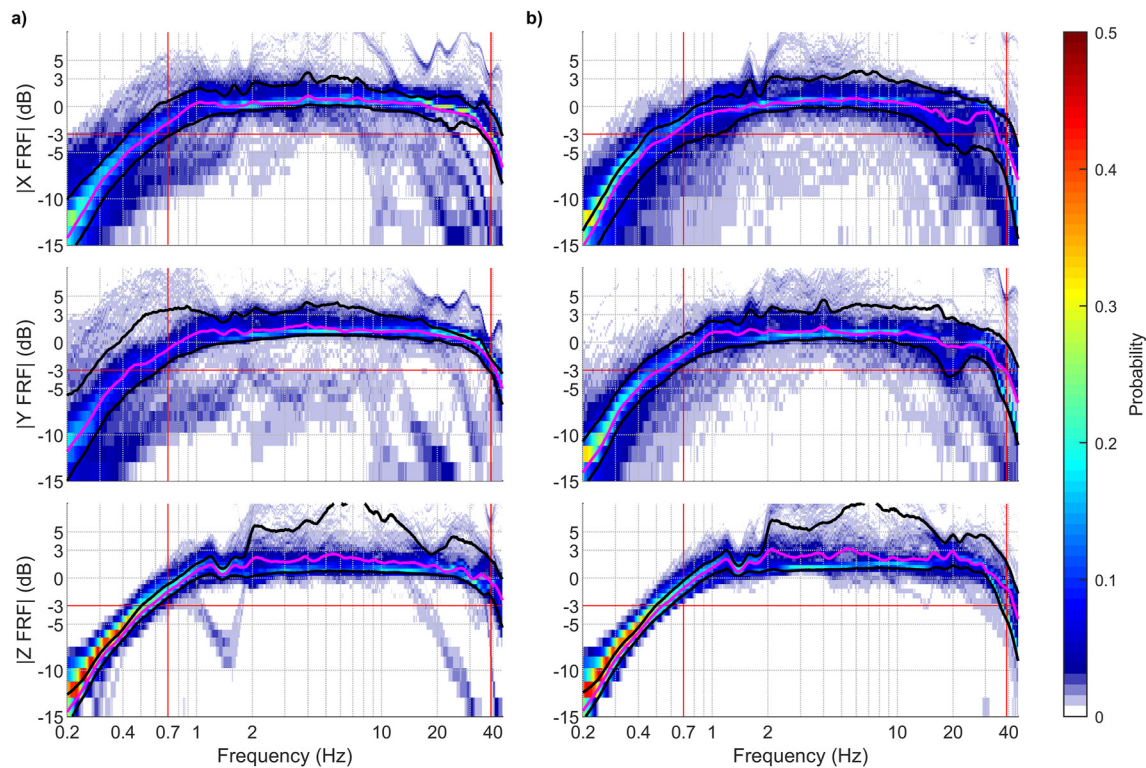


Figure 6. Estimated component-wise spectral ratios for RS3D1 (a) and RS3D2 (b). Z is the vertical component. Ratios are expressed in dB and presented in terms of relative probability. Magenta curve is the median spectral ratio (i.e., 50th percentile), while upper and lower black curves are 75th and 25th percentile, respectively. Red solid lines mark the nominal -3 dB band of the RS3D (Table 1).

percentiles ratios. In addition, red lines limit the -3 dB band of the RS3D, that according to the technical specifications of the V5 release, should span across the 0.7–39 Hz frequency range (Table 1).

It can be noted that the best matching between RS3D and NT20 amplitude responses is observed in a band approximately ranging from 1 to 30 Hz, although the spectral values of the low-cost seismometer are always larger than the Trillium ones (i.e., ratios are always greater than 0 dB), this indicating that the nominal sensitivity of the RS3D may be overestimated. If we consider the median curves, the lower corner of the nominal -3 dB band of the RS3D could be extended down to about 0.55 Hz on average.

4. Discussion and Conclusions

The laboratory tests performed to evaluate the vertical component of 2 RS3Ds in response to extremely high amplitude excitation signals highlighted the non-linear behavior and differences in the FRF magnitude of the tested seismometers, though in presence of different input amplitudes (Figure 4a). Still, the measured -3 dB bandwidth is within the nominal specifications. Anthony et al. (2019) have proposed the lab characterization of the Raspberry Shake 4D, which includes a 0.5 Hz (hyper-damped) vertical component geophone and a 3-component MEMS accelerometer. Though this study is a useful baseline to compare the experimental characterization presented here, some interesting differences can be highlighted. Focusing on the geophone, the authors tested the sensor on vertical shake table and drive the table with a swept sine wave from 0.1 to 10 Hz and 0.015 m/s constant velocity (0-to-peak). They modeled the FRF by using a single-degree-of-freedom oscillator with viscous damping and give the results only in terms of the best-fitting knee frequency (near 0.5 Hz) and of the related damping. On the contrary, our approach allows retrieving the instrument response in the whole band of interest (0.5–40 Hz), highlighting the variability of the FRF within this band and the discrepancy up to about -2 dB between the nominal and the measured FRFs (Figure 4). Moreover, we have identified the non-linear behavior of the instrument versus the input (validated by both the sweep sine and step sine testing), that was neither mentioned nor quantified in any previous studies. In addition, we point out that no idle tones, either

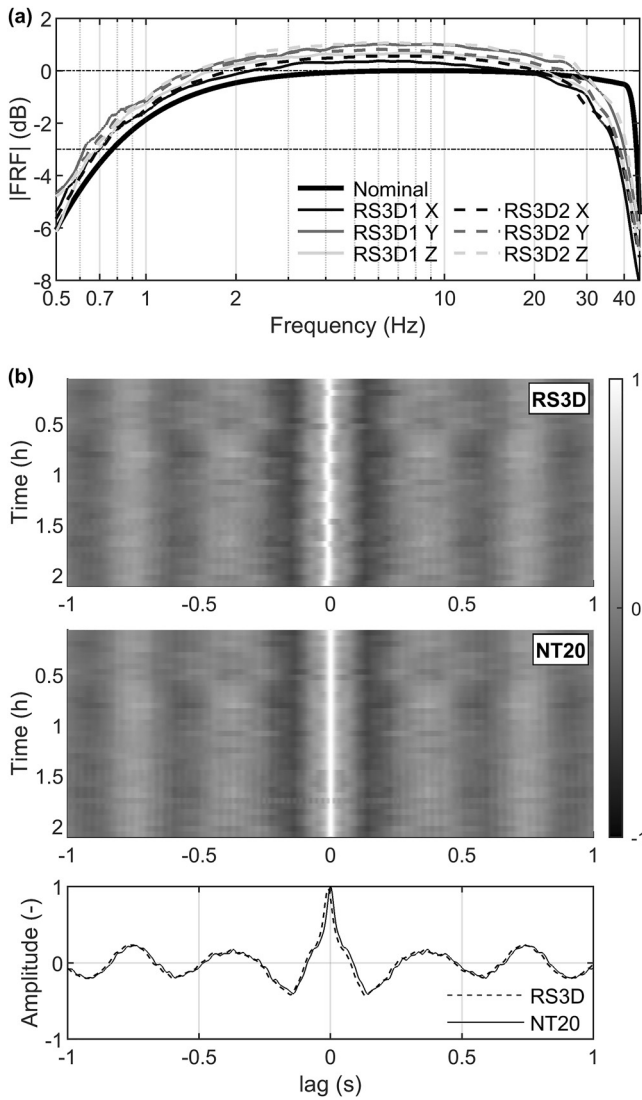


Figure 7. (a) Amplitude frequency response functions obtained in a field test where the same RS3Ds tested in the lab were deployed on asphalt, together with two NT20s, considered as reference. (b) Interferograms obtained by cross-correlating the signals collected by the RS3Ds (top) and NT20s (middle) and the associated mean cross correlation curves (bottom). In the interferograms, single cross correlations are normalized to their maximum value.

low- or high-frequency, are found in RS3D V5, contrary to what has been observed in previous releases or in other units belonging to the Raspberry Shake family (Anthony et al., 2019).

3-component field measurement sessions involving RS3Ds and NT20s (used as reference) benefited from much lower excitation signals. We evaluated that mean rms values of field data as detected by NT20 seismometers are in the range 1–8 $\mu\text{m/s}$, with higher amplitudes generally on the horizontal components, that is approximately three orders of magnitude lower than the excitation amplitudes tested in the lab (Figure 4). The estimated magnitude FRFs extend the -3 dB lower frequency limit down to 0.55 Hz for all the components. We attribute the variance of the computed RS3D/NT20 spectral ratios mainly to differences in coupling between the seismic stations, inaccurate alignment of the two sensors, especially in the horizontal plane, and to non-linear effects affecting the RS3Ds in presence of high-amplitude transients as observed in the lab. The analysis of the estimated PSDs confirms that recorded signals are above the RS3D self-noise level, that has been estimated to range between -150 and -120 dB (rel. $1 \text{ m}^2/\text{s}^4\text{-Hz}^{-1}$) in the 0.5–40 Hz frequency band (Anthony et al., 2019).

In order to better evaluate the RS3D performance in the field, we considered into more detail the test with the seismic stations deployed on asphalt (Figure 5c), thanks to which we have low excitation signals (rms below 3 $\mu\text{m/s}$) and can neglect relevant differences in sensor coupling as well as high-amplitude transients. The processing sequence is the same we used to obtain magnitude FRFs (Figure 6), and, for sake of comparison, spectral ratios are now performed considering the same reference NT20 for both the deployed RS3Ds. The obtained results (Figure 7a) show, as expected, higher FRF values because of lower excitation signals, a good agreement with the nominal response at low frequency and a wider roll-off band at high frequency. Nevertheless, the -3 dB band can still be considered to span approximately from 0.7 to 39 Hz. It can be noticed that there are differences of 0.5 and 0.4 dB (i.e., around 6%) between the components of the same seismometer and between the same component of the two RS3Ds, respectively. With the aim of simulating a SNI test, we constructed two interferograms by cross-correlating the vertical component of signals collected by the RS3Ds and NT20s subdivided in 200 s-windows (Figure 7b). It can be observed that the results are very similar, with a marked peak at zero lag and a sinusoidal trend that are both due to the fact that the computed cross correlations are actually autocorrelations, given the very short offset between the seismic stations. However, the peak of the RS3D interferogram jitters about 10 ms (1 sample) around zero lag because of the limit on the nominal timing accuracy (Table 1). What stated above is also confirmed by considering the average cross correlation curves (Figure 7b), where the peak of the RS3D curve occurs 10 ms before the peak of the NT20 one.

Another field survey that we considered more carefully is the one we performed to monitor four conglomerate rock towers about 100 m high and separated by wide cracks, that are believed to be involved in a lateral spreading phenomenon (Arosio et al., 2019). In more detail, we focus on the two westmost towers (hereafter T1 and T2; Figure 8a) that are known to have their first vibration modes with frequency around 2 Hz. Seismic noise data were collected in late March 2019 by deploying the RS3Ds tested in the lab together with two NT20s (one couple for each monitored tower). All seismic stations were connected to GNSS antennas correctly locked to the GNSS network. The processing sequence was similar to the one used in the asphalt test, but, to evaluate the reliability of the low cost sensors in 3C acquisitions, it was decided to compute the horizontal-to-vertical spectral ratio as a function of azimuth (HVSRA). Accordingly, first the horizontal components are projected along a specific direction, second multitaper estimation is applied to both radial and vertical components after the time series

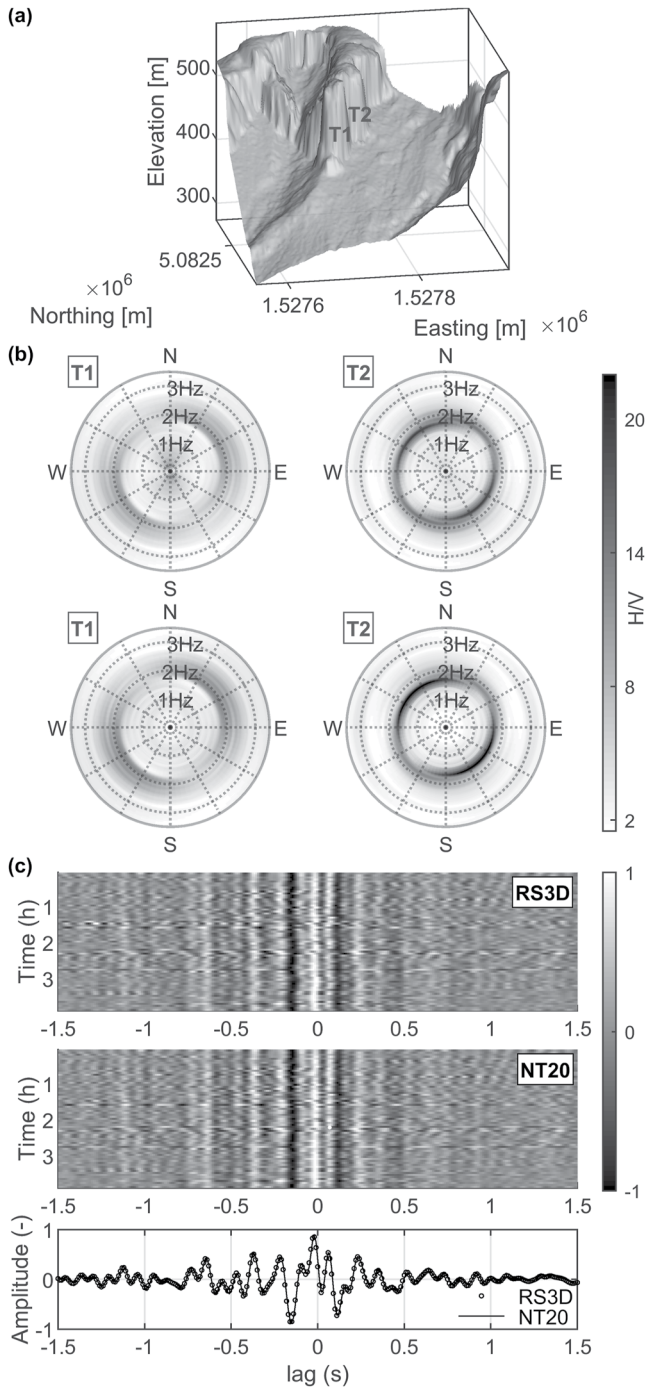


Figure 8. (a) 2×2 m DTM of the investigated area with Towers 1 and 2 in the foreground. (b) HVSRs estimated by RS3Ds (top) and by NT20s (bottom). (c) Interferograms obtained by cross-correlating the signals collected by the RS3Ds (top) and NT20s (middle) and the associated mean cross correlation curves (bottom). In the interferograms, single cross correlations are normalized to their maximum value.

have been subdivided in 200s-time windows, third horizontal-to-vertical spectral ratios (HVSRs) are computed for each time window and, finally, all the HVSRs are averaged using a geometric mean that is most sensitive to low values so as to produce a robust HVSR estimate. This procedure is repeated for several directions in the horizontal plane and yields the HVSR estimate. The first vibration modes for T1 and T2 are found with RS3Ds at 1.68 and 1.93 Hz, respectively, and closely match the outcomes obtained with the NT20 seismometers, both in terms of natural frequencies and vibration directions, the only difference being the peak amplitude, that is about 20% lower for the RS3D (Figure 8b). Also, the interferograms computed in the RS3D -3 dB band to discard high-frequency transients recorded by the NT20s are very similar with again some jittering affecting the RS3D results. The mean cross correlation curves are essentially overlaid (Figure 8c). It is interesting to note that the interferograms are not symmetrical with respect to zero lag and have more energy at negative lags. According to the theory of SNI (Wapenaar et al., 2010), this suggests that seismic noise sources are not evenly distributed around the seismic stations and more seismic energy is traveling from T1 to T2, probably because T1 is more exposed to wind action.

The obtained results confirm that the 3-component recordings of RS3Ds are comparable to the NTS20 ones, despite possible differences in ground coupling between the seismometers, and that the hyper damping is reliable, as the low-cost units correctly identify the resonance frequency of the monitored rock pillars well below the natural frequency of the mounted geophones (i.e., 4.5 Hz). The obtained results, show that, as partial adjustment to what stated by Anthony et al. (2019), the RS3D can be used for—at least shallow—studies using ambient seismic noise.

Regarding RS3D timing accuracy and jittering possibly affecting the computed interferograms, this may have an impact on seismic noise interferometry used, for example, to estimate velocity variations due to saturation changes in the shallow subsurface. According to the theory of CWI (Snieder, 2006)

$$\delta t/t = -\delta v/v$$

where δt is the time perturbation of seismic arrivals in a time window centered in t caused by a homogeneous velocity variation δv in a medium with initial propagation velocity v . The relative velocity variation ($\delta v/v$) is dominated by shear-wave velocity changes (Snieder, 2006) and it is generally much smaller than 10% (e.g., Voisin et al., 2016). Considering commonly found propagation velocities and seismic station distances in shallow SNI surveys, in some instances the lower RS3D timing accuracy may mask the sought velocity variations or yield noisier results. But these issues could be tackled by careful planning of field operations and effective data processing. Of course, any passive seismic survey designed with closely spaced receivers and in presence of high propagation velocities should consider if the timing accuracy could be a limiting factor to obtain meaningful results.

Together with the Raspberry Shake development team (Richard Boaz and Branden Christensen, written comm., 2021–2022), we analyzed the average timing offset of 0.48 s (48 samples) that we found in the field datasets.

Firmware version of our units was updated to the latest release (0.20) and the Linux service daemon `gpsd` (a service process that runs in the background and monitors any GPS receiver attached to the RS3D through the USB port) was updated so that it also looks at the correct USB port for GPS data. We performed additional acquisitions with RS3D and NT20 units placed on the asphalt, but the timing

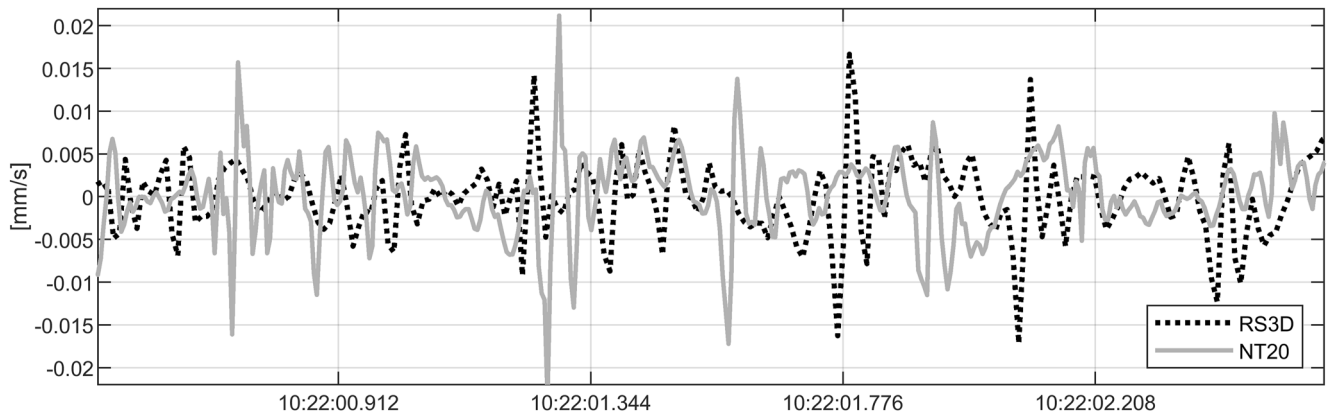


Figure 9. Example of seismic noise collected in the field showing that RS3D data lag NT20 data of approximately 0.5 s. Timing was provided by GPS antennas connected to the units.

offset still persists (Figure 9). Similarly to what has been suggested by other Raspberry Shake users, we believe that our GPS module is not exposing the PPS signal to the Raspberry Pi board. This may happen because it is difficult for a GPS dongle manufacturer to guarantee that the PPS signal is delivered accurately and flawlessly over the USB port due to inaccuracies caused by the inherent delay in the USB interface. The Raspberry Shake team strongly suggests to use the GPS module that is officially offered, since it is configured to deliver the PPS signal over USB to the shared memory slot used by the NTP daemon. As far as the authors are aware, no issues have been reported when Raspberry Shake units are connected to the internet and rely on NTP servers for timing. Finally, we report that timing accuracy between the two tested RS3Ds was found to be ≤ 10 ms (i.e., 1 sample at worst). For sake of completeness, we recall that tests performed by Anthony et al. (2019) to analyze NTP timing accuracy with the accelerometer included in the Raspberry Shake 4D indicate that collected signals always lagged reference ones by two samples (20 ms).

Data Availability Statement

The datasets collected both in the laboratory and in the field, as well as the MatLab routines used to process the data and generate the figures presented in this study are available at Harvard Dataverse repository via <https://doi.org/10.7910/DVN/MAJMEA> with license CC BY-NC-SA 4.0. Additionally, the Incorporated Research Institutions for Seismology (IRIS) nominal response library is available at <https://ds.iris.edu/ds/nrl/> (last accessed February 2023). JEvalResp, a Java utility for evaluating and processing instrument response descriptions, is freely available on IRIS web site (<https://ds.iris.edu/ds/nodes/dmc/software/downloads/jevalresp/>, last accessed February 2023). Raspberry Shake nominal responses may be found at <https://manual.raspberrypi.org/meta-data.html#raspberrypi-shake-rs3> (last accessed February 2023).

References

- Ackerley, N. (2015). Principles of broadband seismometry. In M. Beer, I. A. Kogioumtzoglou, E. Patelli, & S. K. Au (Eds.), *Encyclopedia of earthquake engineering* (pp. 1–35). Springer.
- Aguzzoli, A., Zanzi, L., & Arosio, D. (2021). Seismic noise azimuthal spectral ratios to monitor landslide kinematics. In *Paper presented at NSG2021 27th European meeting of environmental and engineering geophysics*. <https://doi.org/10.3997/2214-4609.202120213>
- Alarcón, M., Soto, P., Hernández, F., & Guindos, P. (2023). Structural health monitoring of South America's first 6-Story experimental light-frame timber-building by using a low-cost Raspberry Shake seismic instrumentation. *Engineering Structures*, 275(B), 115278. <https://doi.org/10.1016/j.engstruct.2022.115278>
- Anthony, R. E., Ringler, A. T., Wilson, D. C., & Wolin, E. (2019). Do low-cost seismographs perform well enough for your network? An overview of laboratory tests and field observations of the OSOP raspberry Shake 4D. *Seismological Research Letters*, 90(1), 219–228. <https://doi.org/10.1785/0220180251>
- Arosio, D. (2023). Seismic noise data and processing software used to test a low-cost 3C seismometer (Version 2) [Dataset and software]. Harvard Dataverse. <https://doi.org/10.7910/DVN/MAJMEA>
- Arosio, D., Longoni, L., Papini, M., Bièvre, G., & Zanzi, L. (2019). Geological and geophysical investigations to analyse a lateral spreading phenomenon: The case study of Torrioni di Rialba, northern Italy. *Landslides*, 16(7), 1257–1271. <https://doi.org/10.1007/s10346-019-01176-w>
- Barzilai, A., VanZandt, T., & Kenny, T. (1998). Improving the performance of a geophone through capacitive position sensing and feedback. In *Paper presented at ASME int. mechanical engineering congress and exposition*.

Acknowledgments

We would like to thank Laura Longoni and Monica Papini for fruitful discussion on seismic investigations of unstable slopes. We are grateful to Francesco Ronchetti, Mauro Soldati, Alessandro Corsini, Marco Mulas, Giuseppe Ciccarese and Vincenzo Critelli at Università degli studi di Modena e Reggio Emilia for their help in planning and performing Ca' Lita and Malta field surveys. We wish to thank Richard Boaz of the Raspberry Shake team for his support on the Raspberry Shake GPS modules.

- Bonnefoy-Claudet, S., Cotton, F., & Bard, P.-Y. (2006). The nature of noise wavefield and its applications for site effects studies. A literature review. *Earth-Science Reviews*, 79(3–4), 205–227. <https://doi.org/10.1016/j.earscirev.2006.07.004>
- Bottelin, P., Baillet, L., Larose, E., Jongmans, D., Hantz, D., Brenguier, O., et al. (2017). Monitoring rock reinforcement works with ambient vibrations: La Bourne case study (Vercors, France). *Engineering Geology*, 226, 136–145. <https://doi.org/10.1016/j.enggeo.2017.06.002>
- Calais, E., Symithe, S., Monfret, T., Deluis, B., Lomax, A., Courboux, F., et al. (2022). Citizen seismology helps decipher the 2021 Haiti earthquake. *Science*, 376(6590), 283–287. <https://doi.org/10.1126/science.abn1045>
- Foti, S., Hollender, F., Garofalo, F., Albarello, D., Asten, M., Bard, P. Y., et al. (2018). Guidelines for the good practice of surface wave analysis: A product of the InterPACIFIC project. *Bulletin of Earthquake Engineering*, 16(6), 2367–2420. <https://doi.org/10.1007/s10518-017-0206-7>
- Garambois, S., Voisin, C., Romero Guzman, M. A., Brito, D., Guillier, B., & Réffloch, A. (2019). Analysis of ballistic waves in seismic noise monitoring of water table variations in a water field site: Added value from numerical modelling to data understanding. *Geophysical Journal International*, 219(3), 1636–1647. <https://doi.org/10.1093/gji/ggz391>
- Hicks, S. P., Verdon, J., Baptie, B., Luckett, R., Mildon, Z. K., & Gernon, T. (2019). A shallow earthquake swarm close to hydrocarbon activities: Discriminating between natural and induced causes for the 2018–2019 Surrey, United Kingdom, earthquake sequence. *Seismological Research Letters*, 90(6), 2095–2110. <https://doi.org/10.1785/0220190125>
- Kleinbrod, U., Burjáněk, J., & Fäh, D. (2017). On the seismic response of instable rock slopes based on ambient vibration recordings. *Earth Planets and Space*, 69(1), 126. <https://doi.org/10.1186/s40623-017-0712-5>
- Konno, K., & Ohmachi, T. (1998). Ground-motion characteristics estimated from spectral ratio between horizontal and vertical components of microtremor. *Bulletin of the Seismological Society of America*, 88(1), 228–241. <https://doi.org/10.1785/BSSA0880010228>
- Larose, E., Carrière, S., Voisin, C., Bottelin, P., Baillet, L., Guéguen, P., et al. (2015). Environmental seismology: What can we learn on earth surface processes with ambient noise? *Journal of Applied Geophysics*, 116, 62–74. <https://doi.org/10.1016/j.jappgeo.2015.02.001>
- Le Breton, M., Bontemps, N., Guillemot, A., Baillet, L., & Larose, E. (2021). Landslide monitoring using seismic ambient noise correlation: Challenges and applications. *Earth-Science Reviews*, 216, 103518. <https://doi.org/10.1016/j.earscirev.2021.103518>
- Lecoq, T., Hicks, S. P., Van Noten, K., Van Wijk, K., Koelemeijer, P., De Plaen, R. S. M., et al. (2020). Global quieting of high-frequency seismic noise due to COVID-19 pandemic lockdown measures. *Science*, 369(6509), 1338–1343. <https://doi.org/10.1126/science.abd2438>
- Lippmann, E., & Gebrande, H. (1983). Eine einfache Methode zur Erweiterung des Meßbereichs elektrodynamischer Seismometer. In *Paper presented at the annual meeting of the German geophysical society*.
- Louie, J. N. (2001). Faster, better: Shear-wave velocity to 100 meters depth from refraction microtremor arrays. *Bulletin of the Seismological Society of America*, 91(2), 347–364. <https://doi.org/10.1785/0120000098>
- Mainsant, G., Larose, E., Brönnimann, C., Jongmans, D., Michoud, C., & Jaboyedoff, M. (2012). Ambient seismic noise monitoring of a clay landslide: Toward failure prediction. *Journal of Geophysical Research*, 117(F1), F01030. <https://doi.org/10.1029/2011JF002159>
- Manconi, A., Coviello, V., Galletti, M., & Seifert, R. (2018). Short communication: Monitoring rockfalls with the raspberry shake. *Earth Surface Dynamics*, 6(4), 1219–1227. <https://doi.org/10.5194/esurf-6-1219-2018>
- McNamara, D. E., & Buland, R. P. (2004). Ambient noise levels in the continental United States. *Bulletin of the Seismological Society of America*, 94(4), 1517–1527. <https://doi.org/10.1785/012003001>
- Nakamura, Y. (2019). What is the Nakamura method? *Seismological Research Letters*, 90(4), 1437–1443. <https://doi.org/10.1785/0220180376>
- Okada, H. (2003). *The microtremor survey method*. Society of Exploration Geophysicists.
- Oome, A. J. A., Janssen, J. L. G., Encica, L., Lomonova, E., & Dams, J. A. A. T. (2009). Modeling of an electromagnetic geophone with passive magnetic spring. *Sensors and Actuators A: Physical*, 153(2), 142–154. <https://doi.org/10.1016/j.sna.2009.04.019>
- Özcebe, A. G., Tigănescu, A., Ozer, E., Negulescu, C., Galiana-Merino, J. J., Tubaldi, E., et al. (2022). Raspberry shake-based rapid structural identification of existing buildings subject to earthquake ground motion: The case study of Bucharest. *Sensors*, 22(13), 4787. <https://doi.org/10.3390/s22134787>
- Park, C. B., Miller, R. D., Ryden, N., Xia, J., & Ivanov, J. (2005). Combined use of active and passive surface waves. *Journal of Environmental & Engineering Geophysics*, 10(3), 323–334. <https://doi.org/10.2113/JEEG10.3.323>
- Snieder, R. (2006). The theory of coda wave interferometry. *Pure and Applied Geophysics*, 163(2), 455–473. <https://doi.org/10.1007/s00024-005-0026-6>
- Stoll, D. (2015). Seismometer, extended response. In M. Beer, I. A. Kougioumtzoglou, E. Patelli, & S. K. Au (Eds.), *Encyclopedia of earthquake engineering* (pp. 3231–3239). Springer.
- Taruselli, M., Aguzzoli, A., Zanzi, L., & Arosio, D. (2020a). Groundwater level monitoring tests with seismic interferometry. In *Paper presented NSG2020 26th European meeting of environmental and engineering geophysics*. online. <https://doi.org/10.3997/2214-4609.202020200>
- Taruselli, M., Aguzzoli, A., Zanzi, L., & Arosio, D. (2020b). Monitoring Ca' Lita landslide by means of the ambient seismic noise. In *Paper presented NSG2020 26th European meeting of environmental and engineering geophysics*. online. <https://doi.org/10.3997/2214-4609.202071088>
- Taruselli, M., Arosio, D., Longoni, L., Papini, M., & Zanzi, L. (2019). Raspberry Shake sensor field tests for unstable rock monitoring. In *Paper presented at 1st conf. on geophysics for infrastructure planning monitoring and BIM*. <https://doi.org/10.3997/2214-4609.201902558>
- Taruselli, M., Arosio, D., Longoni, L., Papini, M., & Zanzi, L. (2021). Seismic noise monitoring of a small rock block collapse test. *Geophysical Journal International*, 224(1), 207–215. <https://doi.org/10.1093/gji/ggaa447>
- Templeton, M. E. (2017). IRIS library of nominal response for seismic instruments [Dataset]. Incorporated Research Institutions for Seismology. <https://doi.org/10.17611/S7159Q>
- Thomson, D. J. (1982). Spectrum estimation and harmonic analysis. *Proceedings of the IEEE*, 70(9), 1055–1096. <https://doi.org/10.1109/PROC.1982.12433>
- Voisin, C., Garambois, G., Massey, C., & Brossier, R. (2016). Seismic noise monitoring of the water table in a deep-seated, slow-moving landslide. *Interpretation*, 4(3), SJ67–SJ76. <https://doi.org/10.1190/INT-2016-0010.1>
- Walter, J. I., Ogwari, P., Thiel, A., Ferrer, F., Woelfel, I., Chang, J. C., et al. (2019). The Oklahoma geological survey statewide seismic network. *Seismological Research Letters*, 91(2A), 611–621. <https://doi.org/10.1785/0220190211>
- Wapenaar, K., Draganov, D., Snieder, R., Campman, X., & Verdel, A. (2010). Tutorial on seismic interferometry: Part 1—Basic principles and applications. *Geophysics*, 75(5), 75A195–75A209. <https://doi.org/10.1190/1.3457445>
- Winter, K., Lombardi, D., Diaz-Moreno, A., & Bainbridge, R. (2021). Monitoring icequakes in East Antarctica with the raspberry shake. *Seismological Research Letters*, 92(5), 2736–2747. <https://doi.org/10.1785/0220200483>